NASA Technical Memorandum 83434
AIAA-83-1201

Experiments in Dilution Jet Mixing

J. D. Holdeman
Lewis Research Center
Cleveland, Ohio

and

R. Srinivasan and A. Berenfeld
The Garrett Turbine Engine Co.
Phoenix, Arizona

Prepared for the
Nineteenth Joint Propulsion Conference
cosponsored by the AIAA, SAE, and ASME
Seattle, Washington, June 27-29, 1983

NASA

EXPERIMENTS IN DILUTION JET MIXING

by J.D. Holdeman

NASA Lewis Research Center
Cleveland, OH 44135

and

R. Srinivasan
A. Berenfeld

The Garrett Turbine Engine Company
Phoenix, AZ 85010

Abstract

This paper presents experimental results which extend previous studies, on the mixing of a single row of jets with an isothermal mainstream in a straight duct, to include flow and geometric variations typical of combustion chambers in gas turbine engines. The principal conclusions reached from these experiments were: 1) at constant momentum ratio, variations in density ratio have only a second-order effect on the profiles; 2) a first-order approximation to the mixing of jets with a variable temperature mainstream can be obtained by superimposing the jets-in-an-isothermal-crossflow and mainstream profiles; 3) flow area convergence, especially injection-wall convergence, significantly improves the mixing; 4) for opposed rows of jets, with the orifice centerlines in-line, the optimum ratio of orifice spacing to duct height is 1/2 of the optimum value for single side injection at the same momentum ratio; and 5) for opposed rows of jets, with the orifice centerlines staggered, the optimum ratio of orifice spacing to duct height is twice the optimum value for single side injection at the same momentum ratio.

Nomenclature

Aj/Am = orifice-to-mainstream area ratio
= (Pi/4)/((S/D)(Ho/D))
Cd = orifice discharge coefficient
D = orifice diameter
Dj = (D)($\sqrt{Cd}$)
DR = jet-to-mainstream density ratio
= (Tm/Tj)
Ho = duct height at injection plane
J = jet-to-mainstream momentum ratio
= (DR)(R)^2
M = jet-to-mainstream
density-times-velocity ratio
= (DR)(R)
Pi = 3.14159
R = jet-to-mainstream velocity ratio
= (Vj/Um)
S = spacing between orifice centers
T = temperature
Tj = jet exit temperature
Tm = mainstream temperature
U = velocity
Um = mainstream velocity
Vj = jet velocity
x = downstream coordinate
= 0 at injection plane
y = cross-stream (radial) coordinate
= 0 at wall
z = lateral (circumferential)
coordinate
= 0 at centerplane

Introduction

Considerations of dilution zone mixing in gas turbine combustion chambers have motivated several previous studies of the mixing characteristics of a row of jets injected normally into a ducted crossflow (references 1 to 11). In reference 12, the effects of separately varying momentum ratio, density ratio, orifice size, and orifice spacing are reviewed, and the relations among these which optimize the mixing are identified, using the empirical model of reference 5. The current study was initiated to extend the available experimental data on the thermal mixing of dilution jets to include geometric and flow variations characteristic of gas turbine combustion chambers.

The experiments reported herein are a direct extension of the experiments in reference 1 on a single row of jets mixing with an isothermal mainstream in a straight duct. Variations on these experiments considered in the present paper include: the role of the density ratio, variable temperature mainstream, flow area convergence, and opposed in-line and staggered injection. A more complete presentation of the experimental results, and discussion of the empirical modeling performed in this study is given in reference 13.

Experimental Considerations

Figure 1 shows a flow schematic of the dilution jet test rig. The mainstream temperature and velocity profiles can be tailored by adjusting the flow to the profile generator upstream of the test section. Dilution air enters the test section through sharp-edged orifices in the test section walls from the top, bottom, or both.

Figure 2 provides more detail on the test sections and orifice configurations used in this study. The height of the test section at the injection plane, Ho, was 10.16 cm for all tests. Orifice plate open areas were varied from 2.5 to 20 percent of the mainstream cross section at the injection location. The primary independent geometric variables are the orifice size, and the spacing between adjacent orifices. These are conveniently expressed in dimensionless form as the ratio of the duct height to orifice diameter, Ho/D, and the ratio of the orifice spacing to duct height, S/Ho. The product of these is the orifice spacing-to-diameter ratio, S/D; also called the pitch-to-diameter ratio (e.g. refs, 9 & 10).

Tests were performed with single-side injection for non-isothermal mainstream conditions, and for both symmetric and injection-wall convergence, at the rate of .5cm/cm. Both single-side and two-side injection tests were performed using the straight duct test section.

The dilution jet mixing characteristics were determined by measuring temperature and pressure distributions with a vertical rake probe, positioned at different axial and lateral stations. This probe had 20 thermocouple elements, with a 20-element total pressure rake, and a 20-element static pressure rake located nominally 5 mm (.05 Ho) on each side of the thermocouple rake. The center-to-center spacing between sensors on each rake was also .05 Ho.

This probe was traversed over a matrix of from 48 to 64 Z-X plane survey locations. The flow field mapping in the z-direction was done over a distance equal to one or one and a half times the hole spacing, S, at intervals of S/10. For most tests, the x-y plane containing the orifice centerline (centerplane) was at the center of the span surveyed; i.e. data surveys were from midplane to midplane.

Measurements in the x-direction were made at up to 5 planes with $0.25 \leq X/Ho \leq 2$. Note that because the designers' objective is to identify dilution zone configurations to provide a desired mixing pattern within a given combustor length, the downstream stations of interest are defined in intervals of the duct height at the injection location, Ho, rather than the orifice diameter, D.

Results and Discussion

The measured gas temperature distributions are presented in non-dimensional form as:

$$\text{THETA} = \frac{(Ta - T)}{(Ta - Tj)}$$

Note that THETA = 1 if the local temperature is equal to the jet temperature, and THETA = 0 if the local temperature is equal to the mainstream temperature.

The temperature field results are presented in three-dimensional oblique views and as isotherm contours of the temperature difference ratio, THETA. Typical examples of these are shown in figure 3. In these plots the temperature distribution is shown in planes normal to the main flow direction. The coordinates y and z are, respectively, normal to and along the orifice row in this constant X plane. For clarity and consistency of the visual presentation, the THETA distributions are shown over a 2S span in the z-direction, with the plane between jets, the midplane, at the edge of the oblique and contour plots.

Since for most tests, data were obtained over a span of only one orifice spacing, symmetry was assumed where necessary, and the data were reflected across the midplane or centerplane as appropriate. In figures 3a and 3b, the right half of each figure is a reflection of the left (with slight differences due to the contour plotting routine). In figure 3c, the data were obtained from centerplane to centerplane, and the differences between the right and left halves of the figure may be due to differences in flow through adjacent orifices and/or to a slight misalignment between the flow and geometric centerplanes.

The y and z coordinates are shown to scale in the duct cross-section schematics on the right of each row in figure 3. Note the fourfold decrease in the width of the flow region shown from S/Ho=1 in the top row to S/Ho=.25 in the bottom row. The profiles and contours in this figure show the relationship between orifice spacing and momentum ratio that gives optimum mixing for one-side injection, independent of orifice diameter (refs. 2, 5, and 12). This can be stated as:

$$(S/Ho)_{OPT} = \frac{2.5}{\text{SQRT}(J)}$$

The following paragraphs will present the experimental results for single-side injection tests with (separately) a non-isothermal mainstream flow, symmetric and injection-wall convergence, and opposed in-line and staggered injection in a straight duct. In addition to variations with geometry, the distributions are examined in terms of the flow variables DR, R, M, and J, which are respectively the density ratio, velocity ratio, density-times-velocity ratio, and the momentum ratio.

Density Ratio

Figure 4 shows the effect of density ratio on the THETA distributions. These profiles are for an orifice configuration with S/Ho=.5 and Ho/D=8, for three different

flow conditions. For each of these, profiles are shown at downstream distances of X/Ho =.5, 1, and 2 from left to right. The profiles in the top row are for hot jets and an ambient mainstream, whereas the middle and bottom rows are for ambient jets and a hot mainstream.

In the top and middle rows, the momentum ratios are similar, and the profiles are similar, even though the density ratio is .75 in the top row, and 2.2 in the middle row. The slightly smaller THETA levels in the top row are a result of the smaller jets-to-mainstream flow ratio in the hot jets case. In contrast to these, the profiles in the bottom row show over-penetration, as a result of an approximately four-times larger momentum ratio. Note however that the jet-to-mainstream velocity ratios are about the same for the hot-jets/ambient-mainstream case in the first row, and the ambient-jets/hot-mainstream case in the bottom row.

Figure 5 shows a similar comparison for an orifice plate with the same orifice-spacing-to-duct-height ratio (S/Ho), but with larger holes. The hot-jets/ambient-mainstream and ambient-jets/hot-mainstream cases in the top and bottom rows respectively have nearly equal density-times-velocity ratios, but are are very different due to the large difference in their momentum ratios. The top and middle rows show that the THETA distributions become more similar as the momentum ratios approach equality.

Variable Temperature Mainstream

The influence of a non-isothermal mainstream flow on the profiles for S/Ho=.5, Ho/D=4, with J=22 is shown in figure 6. In this figure, the hottest temperature in the mainstream for each case was used as Tm in the definition of THETA.

The isothermal mainstream 'control' case in the top row is the middle row from figure 5. In the center row in figure 6 the upstream profile (left frame) is coldest near the injection wall, whereas in the bottom row, the upstream profile (left frame) is coldest near the opposite wall.

The shape of these distributions suggests modelling them as a superposition of the upstream profile and the jets-in-an-isothermal-mainstream THETA distributions. This gives only a crude approximation however, as there is considerable cross-stream transport of mainstream fluid due to the blockage, and this is not accounted for in superimposing the distributions.

Flow Area Convergence

The effect of flow area convergence on the temperature profiles for S/Ho=.5, Ho/D=4, with J=26 is shown in figure 7. The profiles in the top row are from the straight-duct test which was used as the control case in the previous figure also. Here, as in the non-isothermal mainstream tests, the jets were injected from the top wall.

The profiles in the middle row are for a test section which converges symmetrically to 1/2 of the injection-plane height (Ho) in a downstream distance equal to 1 Ho (i.e. .5cm/cm). At all downstream locations, these profiles are more uniform than the corresponding straight-duct profiles. Even more of an effect is seen in the distributions in the bottom row. The area convergence here is the same as in the middle row, but it is asymmetric, with all of the turning on the injection wall. This has a dramatic effect in creating more uniform temperature distributions, in both the transverse and lateral directions.

Opposing Rows of Jets

The remainder of this paper will present the experimental results for two-side injection from opposing rows of jets, with: 1) the jet centerlines on top and bottom directly opposite each other; and 2) the jet centerlines on top and bottom staggered in the z (circumferential) direction. The results of these tests are shown and compared with the single-side results in figures 8 to 13. For each case, a duct cross-section is shown to scale to the left of the data.

Opposed Jet Injection. Figure 8 shows single-side and opposed jet injection cases at a constant orifice diameter (Ho/D=8), for momentum ratios of approximately 25. For this momentum ratio, an appropriate orifice spacing to duct height ratio for optimum single-side mixing is .5 (references 2 & 5), as can be seen in figure 3 and in the profiles in the top row of figure 8.

For opposed jet injection, with equal momentum ratios on both sides, the effective mixing height is half the duct height, based on the result in reference 3 that the effect of an opposite wall is similar to that of the plane of symmetry in an opposed jet configuration. Thus the appropriate orifice spacing to duct height ratio for opposed jet injection at this momentum ratio is S/Ho=.25. These profiles are shown in the bottom row, and the two streams do indeed mix very rapidly. Note that the jet to mainstream flow ratio is four-times greater in the opposed jet case than in the single-side case.

Figure 9 shows a comparison between single-side and opposed jet injection cases at the same momentum ratio, in which the orifice areas, and hence the jet-to-mainstream flow ratio is constant. Here the opposed jet case requires twice as many holes in the row, at one half the diameter, compared to the optimum single-side case.

Figures 10 and 11 show a similar relationship between single-side and opposed jets, for a nominal momentum ratio of 7, as figures 8 and 9 showed for a momentum ratio of 25. Note that because the momentum ratio is smaller, the S/Ho values in figures 10 and 11 are larger than the corresponding values in figures 8 and 9 (see e.g. fig. 3 and refs. 2, 5, and 12).

Staggered Jet Injection. Finally, figures 12 and 13 show comparisons between single-side and staggered jet injection for momentum ratios of 25 and 105 respectively. Since for opposed injection, it was found that the effective mixing height was half of the duct height, it would seem appropriate to assume for staggered jets that the effective orifice spacing would be half the actual spacing.

This hypothesis is verified by the rapid mixing of the two streams in the bottom row of profiles in figures 12 and 13. In both figures the orifice spacing for the staggered jets is twice the appropriate value for one-side injection at the given momentum ratio. That is, a configuration that optimizes mixing in a one-side configuration, performs even better when every other orifice is moved to the opposite wall.

Summary of Results

The principal conclusions from the experimental results presented herein are:

1) The jet-to-mainstream momentum ratio is the most important operating variable influencing the jet penetration and mixing. At constant momentum ratio, variations in density ratio have only a second-order effect on the profiles.

2) A first-order approximation to the mixing of jets with a variable temperature mainstream can be achieved by superimposing the jets-in-an-isothermal-mainstream and upstream profiles.

3) Flow area convergence, especially injection wall convergence, significantly improves the mixing.

4) For opposed rows of jets, with the orifice centerlines in-line, the optimum ratio of orifice spacing to duct height is one-half of the optimum value for single-side injection at the same momentum ratio.

5) For opposed rows of jets, with the orifice centerlines staggered, the optimum ratio of orifice spacing to duct height is double the optimum value for single-side injection at the same momentum ratio.

References

1. Walker, R.E. and Kors, D.L., "Multiple Jet Study Final Report," NASA CR-121217, June 1973.

2. Holdeman, J.D., Walker, R.E., and Kors, D.L., "Mixing of Multiple Dilution Jets with a Hot Primary Airstream for Gas Turbine Combustors," AIAA Paper 73-1249, Nov. 1973.

3. Kamotani, Y. and Greber, I, "Experiments on Confined Turbulent Jets in Cross Flow," NASA CR-2392, Mar. 1974.

4. Walker, R.E. and Eberhard, R.B.: Multiple Jet Study Data Correlations. NASA CR-134796, 1975.

5. Holdeman, J.D. and Walker, R.E., "Mixing of a Row of Jets with a Confined Crossflow," AIAA Journal, vol.15, no.2, Feb.1977, pp.243-249.

6. Cox, G.B. Jr., "Multiple Jet Correlations for Gas turbine Engine Combustor Design," Journal of Engineering for Power, Vol. 98, No. 2, 1976, pp.265-273.

7. Cox, G.B. Jr., "An Analytical Model for Predicting Exit Temperature Profile from Gas Turbine Engine Annular Combustors," AIAA Paper 75-1307, Sept. 1975.

8. Riddlebaugh, S.M., Lipshitz, A., and Greber, I., "Dilution Jet Behaviour in the Turn Section of a Reverse-Flow Combustor," AIAA Paper 82-0192, Jan. 1982.

9. Khan, Z.A., McGuirk, J.J., and Whitelaw, J.H., "A Row of Jets in Crossflow," Fluid Dynamics of Jets with Application to V/STOL, AGARD-CP-308, Technical Editing and Reproduction. London, 1982.

10. Atkinson, K.N., Khan, Z.A., and Whitelaw, J.H., "Experimental Investigation of Opposed Jets Discharging Normally into a Cross-stream," Journal of Fluid Mechanics, Vol.115, 1982, pp.493-504.

11. Mittig, S.L.K, Elbahar, O.M.F., and Noll, B.E.: Temperature Profile Development in Turbulent Mixing of Coolant Jets with a Confined Hot Cross-Flow," ASME Paper No. 83-GT-39, Mar. 1983.

12. Holdeman, J.D., "Perspectives on the Mixing of a Row of Jets with a Confined Crossflow," AIAA Paper 83-1200, June 1983.

13. Srinivasan, R., Berenfeld, A., and Mongia, H.C., "Dilution Jet Mixing Phase I Report," Garrett Turbine Engine Co., Phoenix, Ariz., Garrett-21-4302, Nov. 1982. (NASA CR-168031).

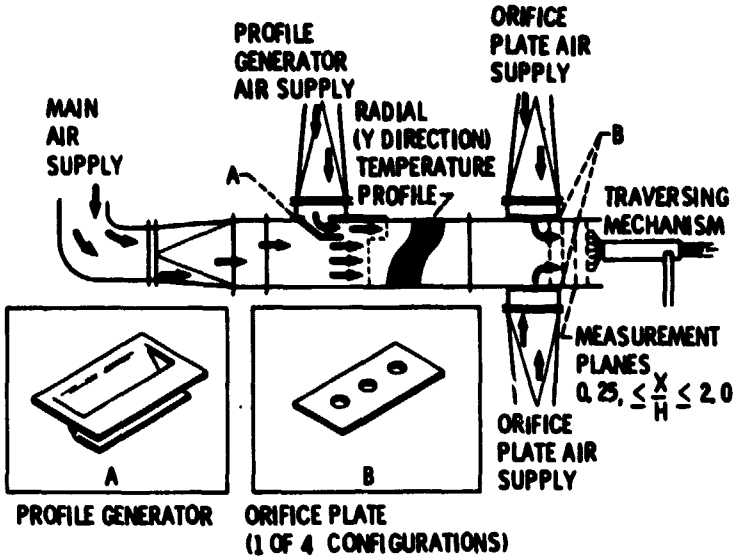

Figure 1. - Dilution Jet Mixing Flow Schematic.

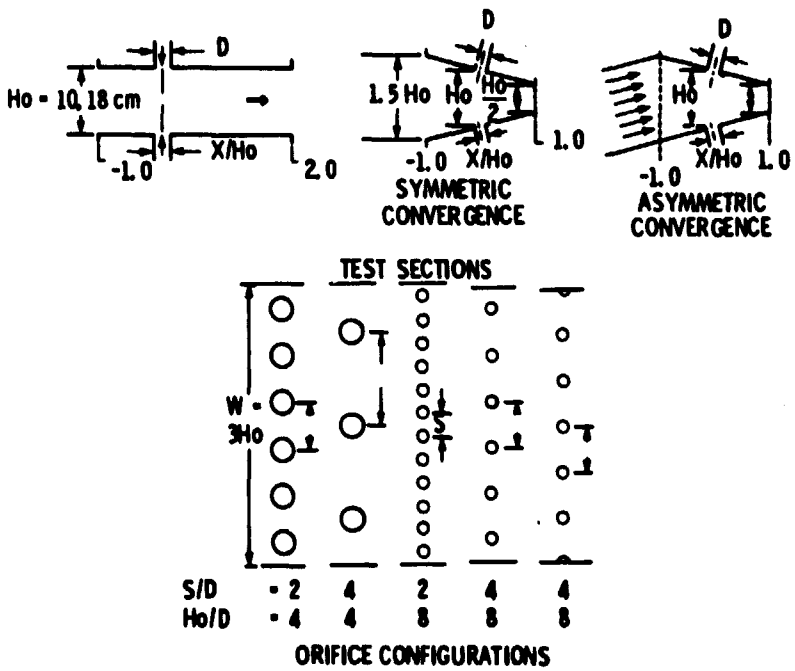

Figure 2. - Test Sections and Orifice Configurations.

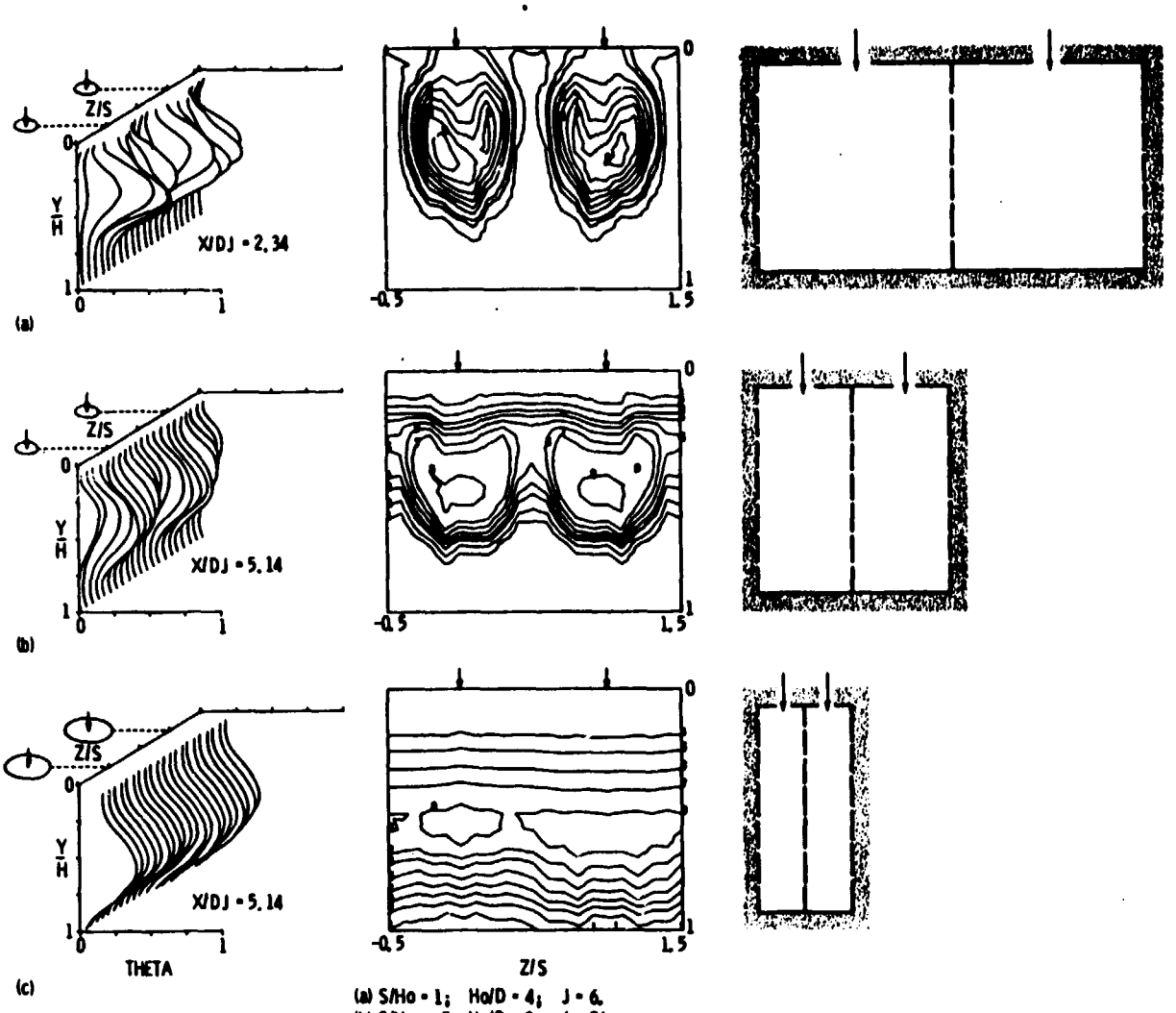

(a) S/Ho = 1; Ho/D = 4; J = 6.
(b) S/Ho = .5; Ho/D = 8; J = 26.
(c) S/Ho = .25; Ho/D = 8; J = 108.

Figure 3. - Typical oblique profile plots and isotherm contours at X/Ho = .5.

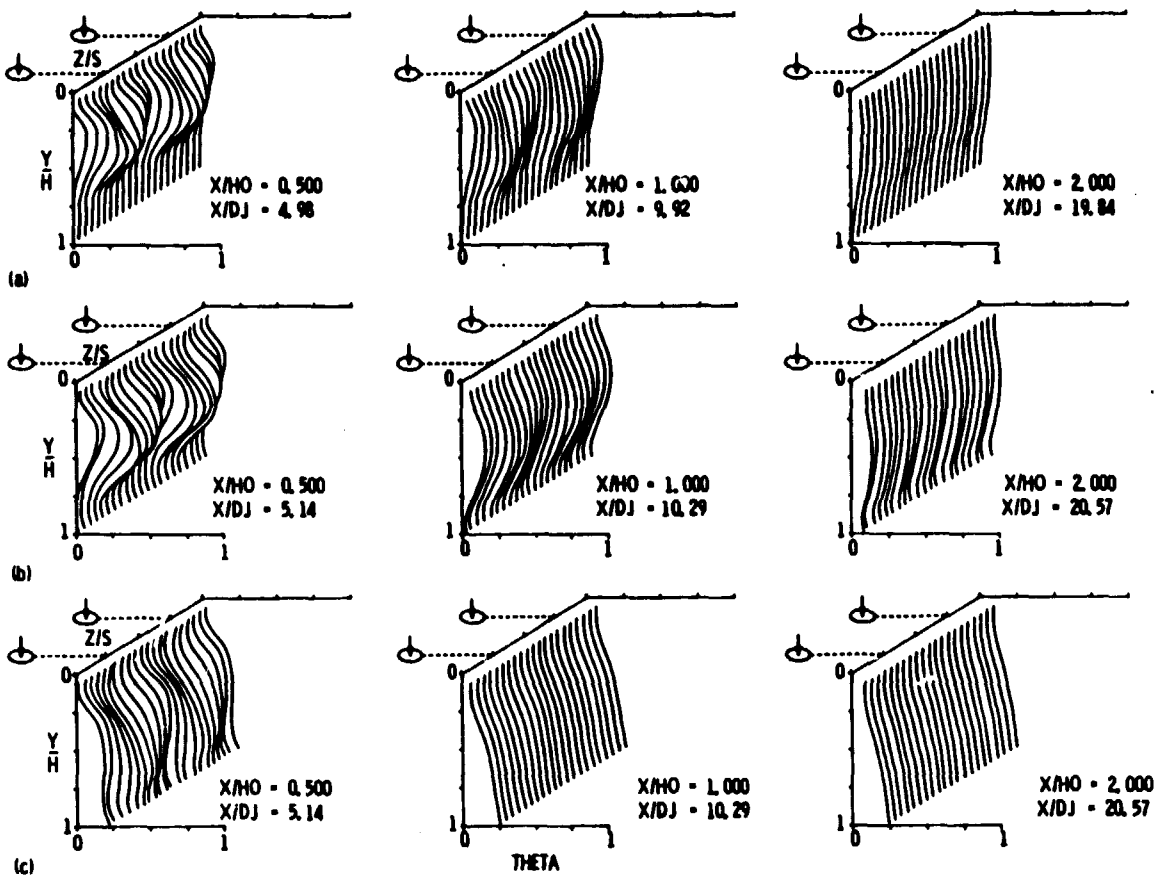

(a) Hot jets - ambient mainstream; DR = .75, J = 31, R = 6.4.
(b) Ambient jets - hot mainstream; DR = 2.2, J = 26, R = 3.5.
(c) Ambient jets - hot mainstream; DR = 2.3, J = 109, R = 6.9.

Figure 4. - Effect of density ratio on temperature profiles (S/Ho = .5, Ho/D = 8).

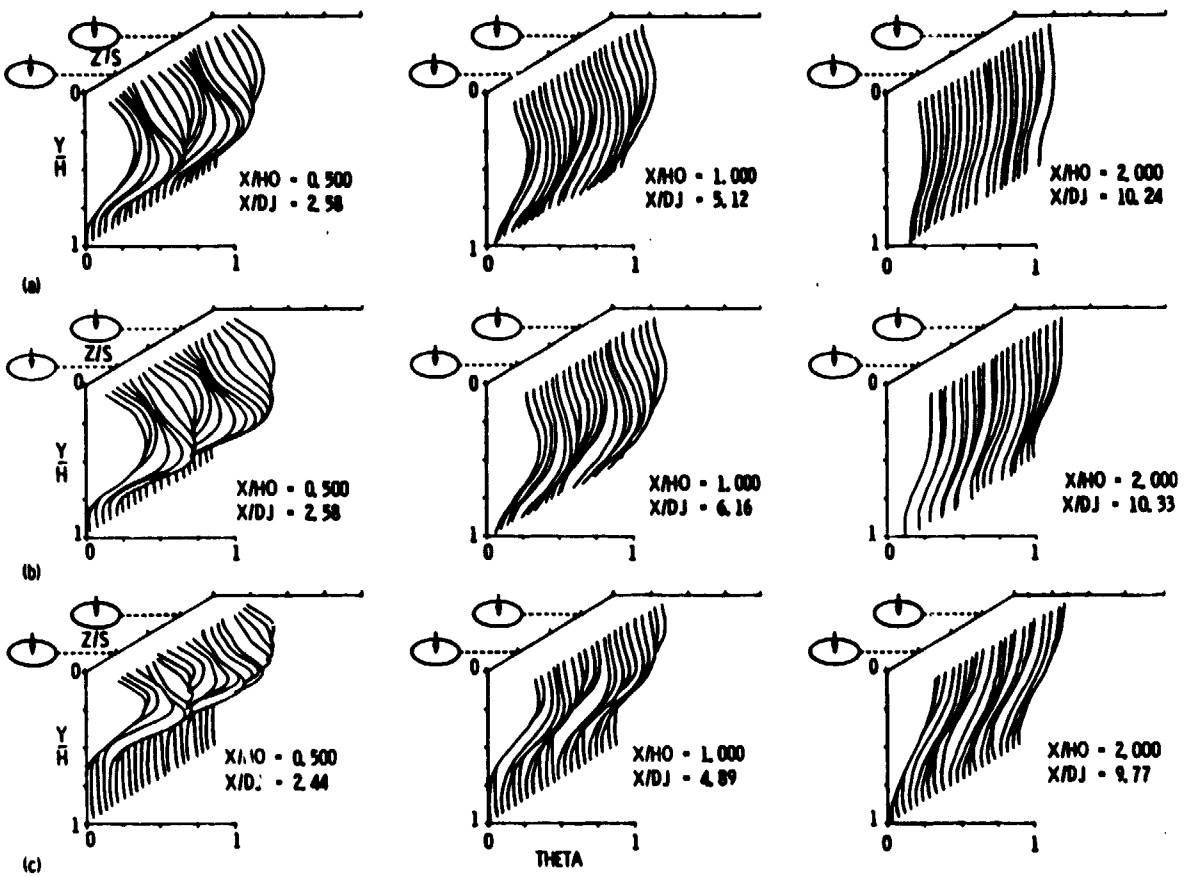

(a) Hot jets - ambient mainstream; DR = .62, J = 31, M = 3.8.
(b) Ambient jets - hot mainstream; DR = 2.1, J = 21.6, M = 6.3.
(c) Ambient jets - hot mainstream; DR = 2.1, J = 5.7, M = 3.2.

Figure 5. - Effect of density ratio on temperature profiles (S/Ho = .5, Ho/D = 4).

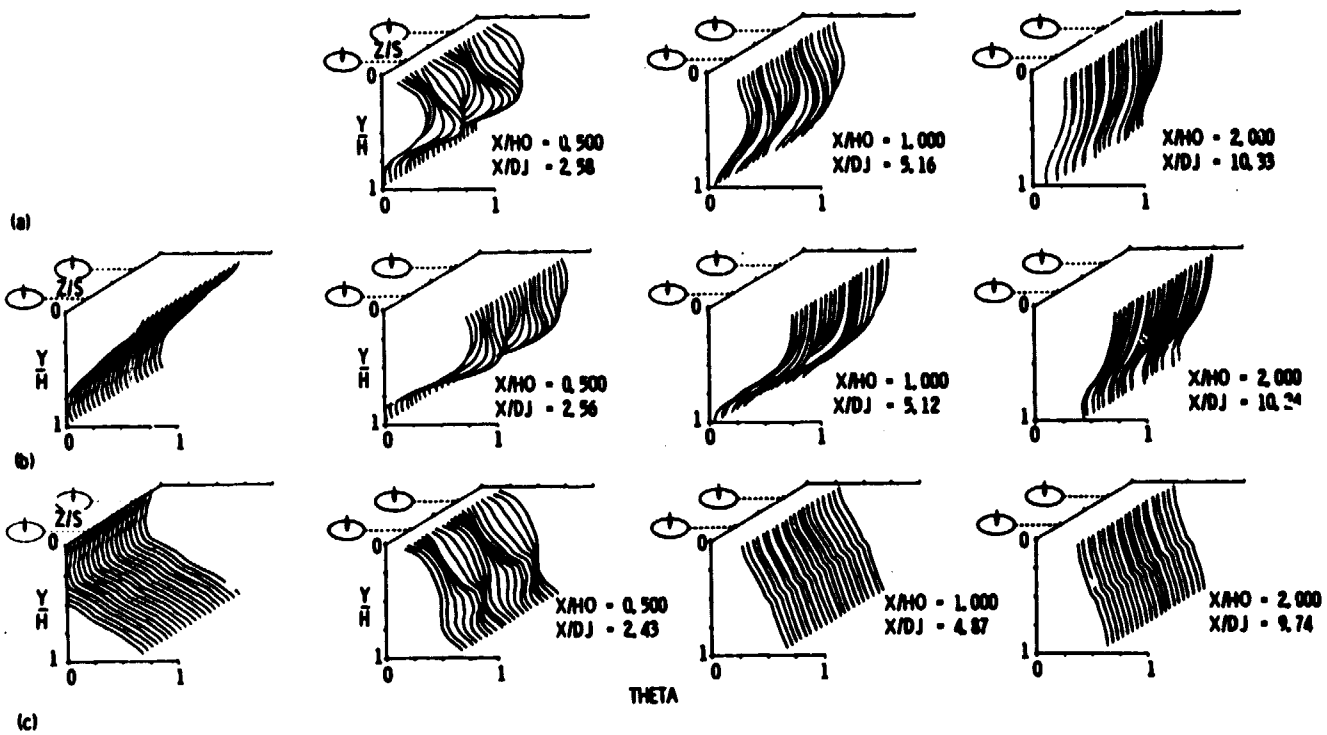

(a) Isothermal mainstream; J = 21.6.
(b) Top cold; J = 22.6
(c) Top hot; J = 22.1.

Figure 6. - Influence of non-isothermal mainstream on temperature profiles (S/Ho = .5, Ho/D = 4).

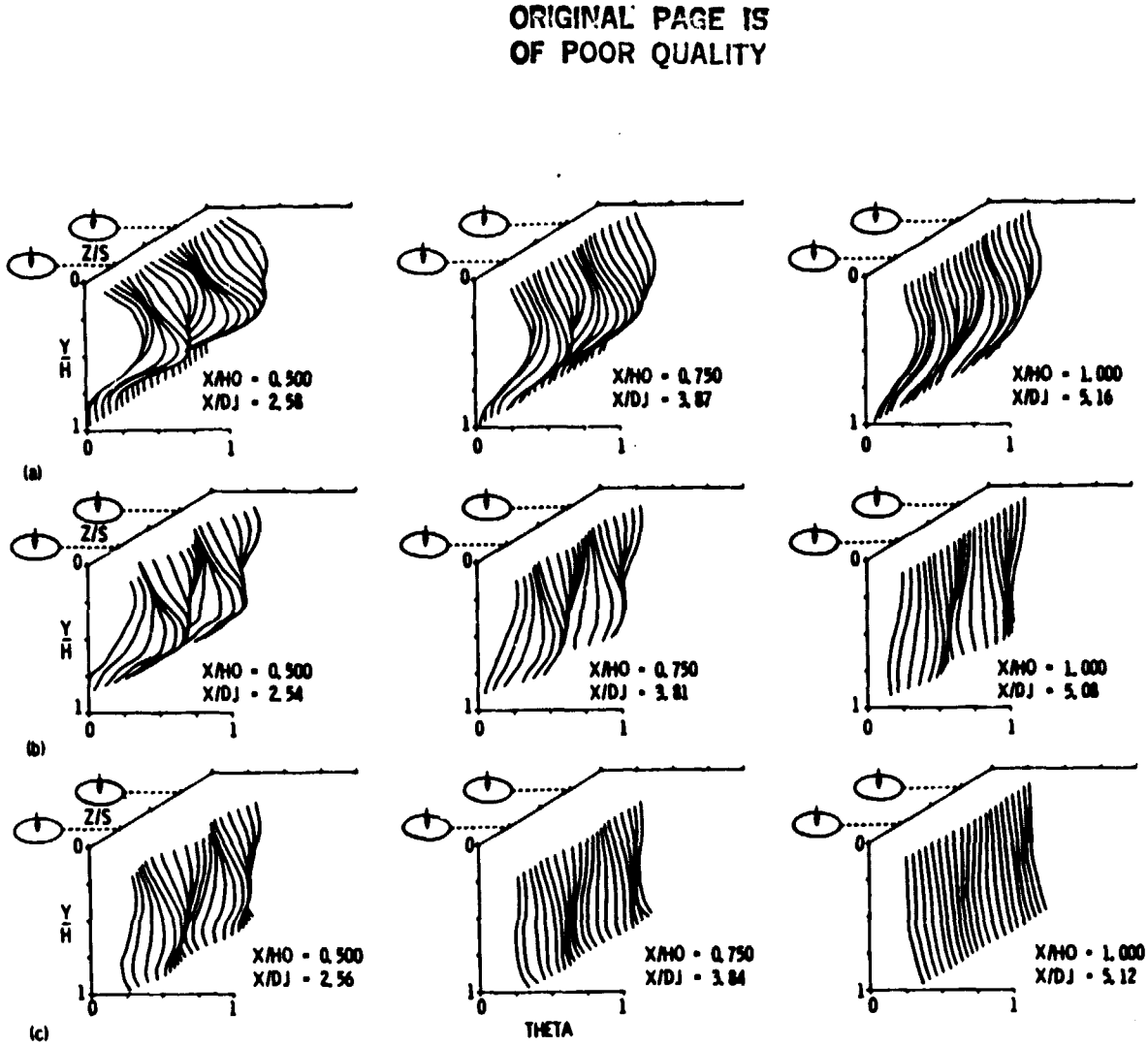

(a) Straight duct; J = 21.6.
(b) Symmetric convergence (.5 cm/cm); J = 26.7.
(c) Injection wall converging (.5 cm/cm); J = 26.4.

Figure 7. - Influence of flow area convergence on temperature profiles (S/Ho = .5, Ho/D = 4).

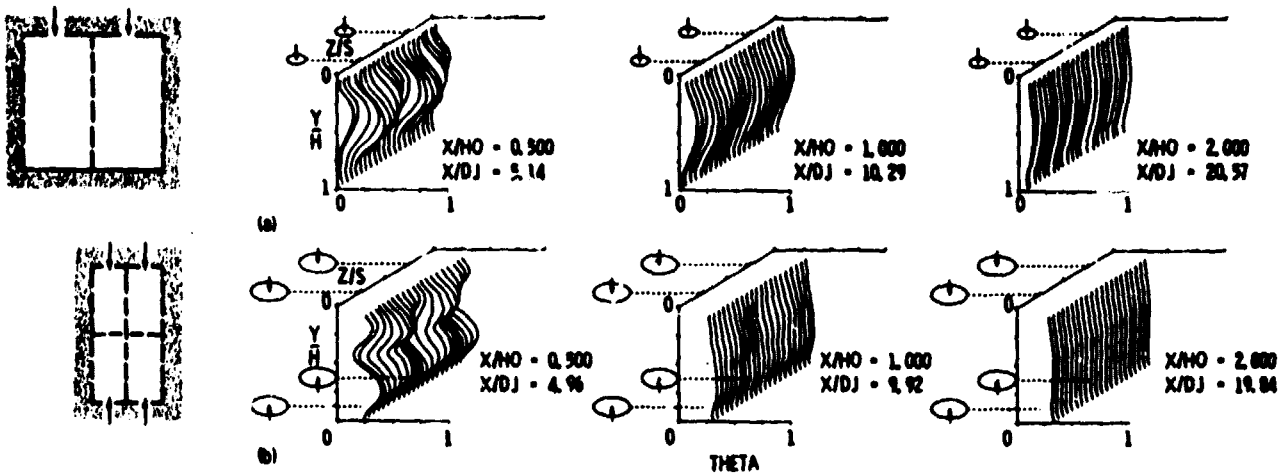

(a) Single-side (top) injection; J = 26.3, S/Ho = .5.
(b) Two-side (opposed) injection; J = 25, S/Ho = .25.

Figure 8. - Comparison between single-side and opposed jet injection (Ho/D = 8).

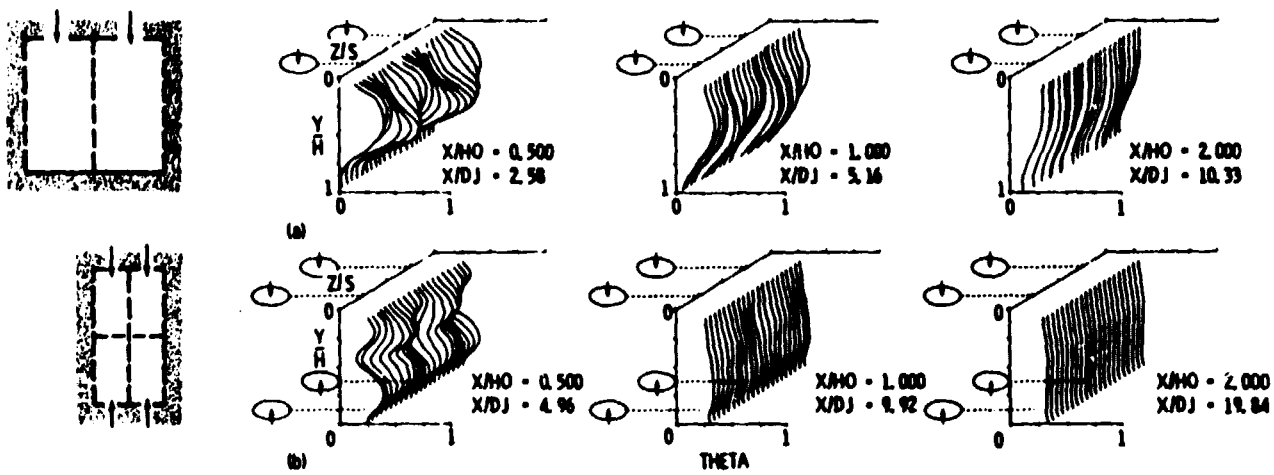

(a) Single-side (top) injection; J = 21.6, S/Ho = .5, Ho/D = 4.
(b) Two-side (opposed) injection; J = 25, S/Ho = .25, Ho/D = 8.

Figure 9. - Comparison between single-side and opposed jet injection (Aj/Am = .11).

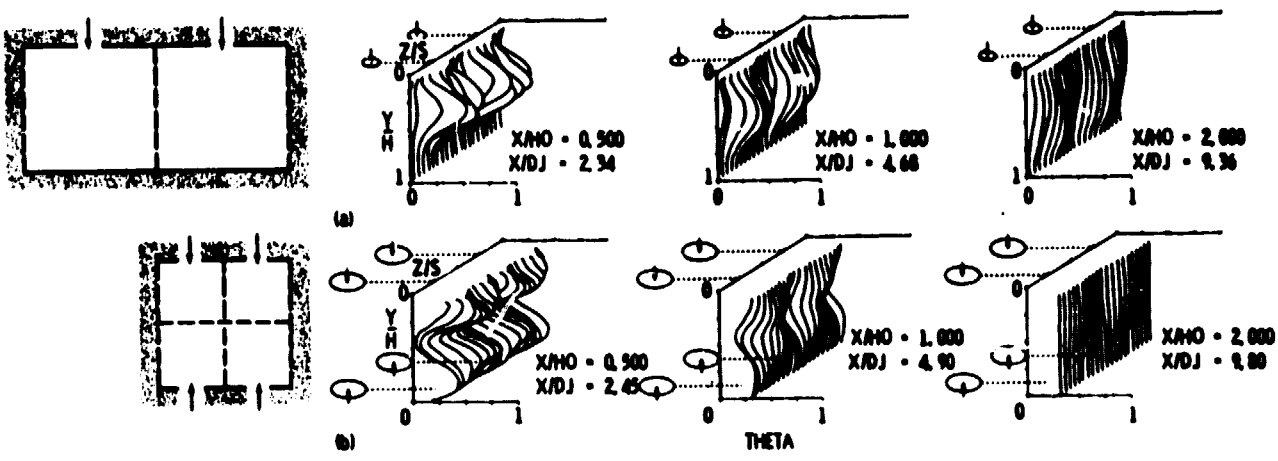

(a) Single-side (top) injection: J = 6.1, S/Ho = 1.
(b) Two-side (opposed) injection: J = 6, S/Ho = .5.

Figure 10. - Comparison between single-side and opposed injection (Ho/D = 4).

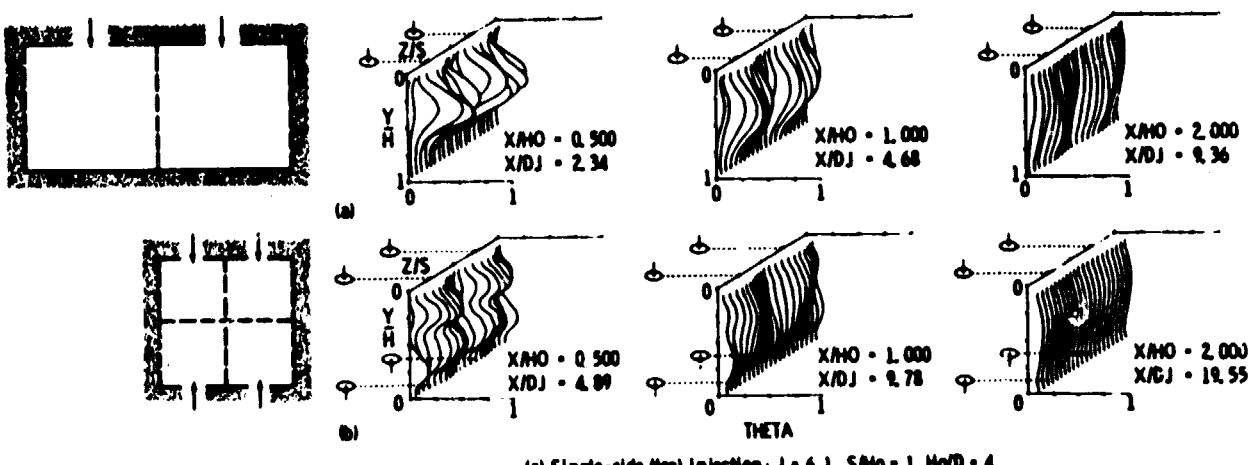

(a) Single-side (top) injection: J = 6.1, S/Ho = 1, Ho/D = 4.
(b) Two-side (opposed) injection: J = 7.8, S/Ho = .5, Ho/D = 8.

Figure 11. - Comparison between single-side and opposed jet injection (Aj/Am = .05).

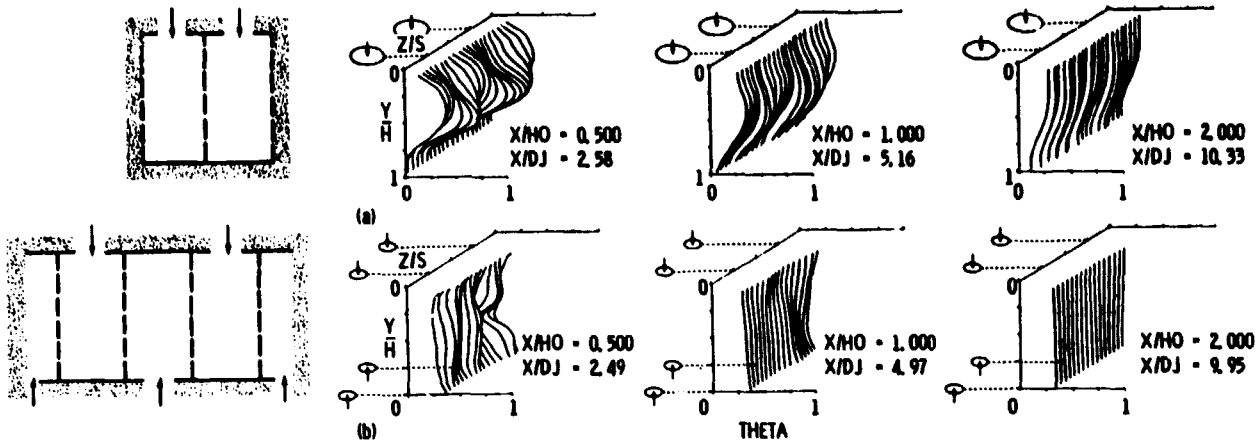

(a) Single-side (top) injection: J = 21.6, S/Ho = .5.
(b) Two-side (staggered) injection: J = 26.4, S/Ho = 1.

Figure 12. - Comparison between single-side and staggered jet injection (Ho/D = 4; Aj/Am = .1).

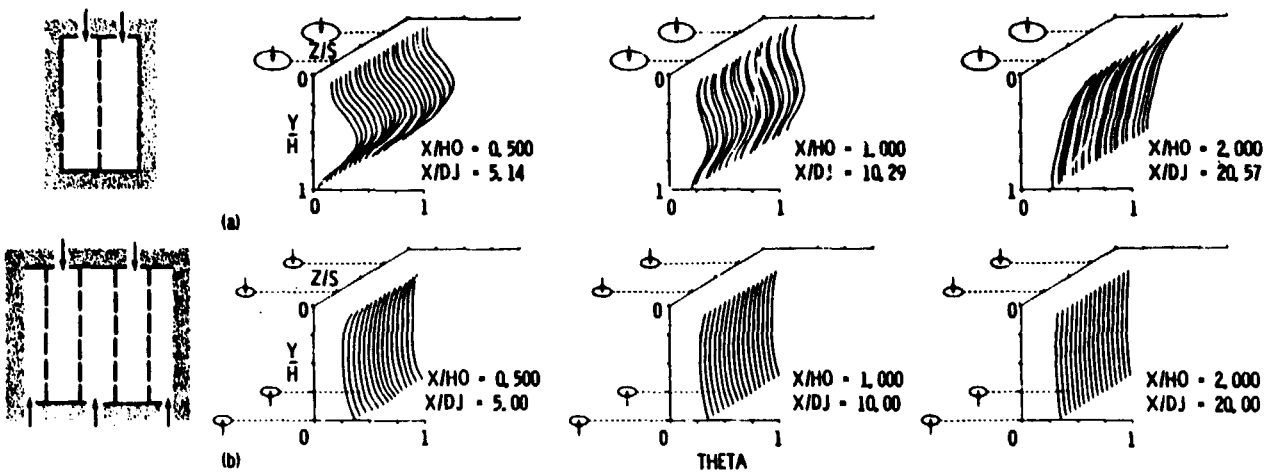

(a) Single-side (top) injection: J = 107.8, S/Ho = .25.
(b) Two-side (staggered) injection: J = 103.1, S/Ho = .5.

Figure 13. - Comparison between single-side and staggered jet injection (Ho/D = 8; Aj/Am = .05).